Journal of Molecular Structure 1221 (2020) 128772

Contents lists available at ScienceDirect

Journal of Molecular Structure

journal homepage: http://www.elsevier.com/locate/molstruc

The novel two step synthesis of CuO/ZnO and CuO/CdO nanocatalysts for enhancement of catalytic activity

A. Sankaran [a], K. Kumaraguru [b, *]

[a] Department of Marine Engineering, Mohamed Sathak Engineering College, Kilakarai, 623806, India
[b] Department of Petrochemical Technology, University College of Engineering, BIT Campus, Anna University, Tiruchirappalli, 620024, India

ARTICLE INFO

Article history:
Received 30 January 2020
Received in revised form
19 June 2020
Accepted 25 June 2020
Available online 1 July 2020

Keywords:
Nanocomposites
Two-step process
Structural
Optical studies
Catalytic activity

ABSTRACT

In the present investigation, Copper oxide (CuO)/Zinc oxide (ZnO) and CuO/cadmium oxide (CdO) nanocomposites (NCs) were fabricated by a simple two-step process involving co-precipitation technique and hydrothermal approach for the first time. The Powder X-ray Diffraction (PXRD) pattern demonstrates the existence of monoclinic, hexagonal and cubic phase structure of CuO/ZnO and CuO/CdO NCs. The absorption spectrum of the material was obtained via UV–Visible Spectroscopy and the band-gap value is calculated using Tauc's relation as 1.7 eV, 2.8 eV and 2.75 eV respectively for pure, CuO/ZnO and CuO/CdO NCs. The FESEM images gave the spherical and stone-like morphologies in the prepared CuO/ZnO and CuO/CdO NCs. At room temperature, CuO/ZnO and CuO/CdO NCs act as superior catalyst for the reduction of Rhodamine B (RhB) and Malachite Green (MG) dyes and degradation efficiency attained to be 77.26%, 73.15% for RhB and 79.82%, 74.69 for MG, respectively.

1. Introduction

In the current decade, wastewater treatment has more attention due to the increase in the absorption of toxic pollutants like organic dyes, pharmaceuticals, microbes, etc. In the waste release [1]. Hence, nowadays various technologies are existing in wastewater treatment for the removal of inorganic and organic dyes. To overcome this problem, nanotechnology is an emerging application to solve the wastewater treatment due to their large surface area to volume ratio of nanomaterials [2]. Among nanotechnology-based process for removing organic pollutants, the catalytic process is one of the most efficient, cost-effective and environment-friendly [3]. Generally, semiconductor catalysts (TiO_2, ZnO, CuO, ZnS, CdO, Ta_2O_5, WO_3, and CdS, etc) act as the promising material for wastewater treatment and degradation of organic and inorganic pollutants in water [3]. Among these, copper oxide (CuO) acts as the important semiconductor material owing to its unique properties like p-type and narrow bandgap. By these unique properties, CuO material used as numerous applications such as solar cell, photocatalysis, catalysis, magnetic storage media, gas sensors, PN junction diode, varistors, detectors and lithium-ion battery applications [4–6]. On the other hand, the n-type semiconductor of zinc oxide (ZnO) has a wide bandgap (3.37 eV) with high excitonic binding energy (~60 meV). Due to this property, ZnO material has been used as various applications like biosensors, gas sensors, nanogenerators and varistors [7,8]. In addition, Cadmium oxide (CdO) is an n-type semiconductor material and it has a wide range of applications such as solar cells, phototransistors, electroplating baths, chemical sensors, liquid crystal displays, transparent electrodes, IR detectors and gas sensors [9]. The semiconductor metal oxides were synthesized via various approaches like sol-gel method, auto combustion method, sonochemical method, wet chemical method, co-precipitation method and thermal decomposition method, etc [10]. Among them, the co-precipitation method is one of the most flourishing techniques for synthesizing the materials and this method is an efficient pre-concentration technique for tracing heavy metal ions. In addition, the shape and size of the particles can be controlled by varying pH medium [1,3]. As well as, various types of nanostructures were developed by a hydrothermal approach owing to its narrow crystallite size distribution and low aggregation level [7].

In a modern trend, new composite materials were fabricated by various researchers due to support of innovative direction for research and applications [11]. Hence, CuO-based nanocomposites were recently developed in current research for catalytic degradation of organic dyes such as Methylene blue, Malachite green,

* Corresponding author.
E-mail address: kumaraguruautt@gmail.com (K. Kumaraguru).

https://doi.org/10.1016/j.molstruc.2020.128772
0022-2860/

Methyl orange and 4-nitrophenol [12–19]. In this connection, Jayapriya et al. fabricated MgO rice/ZnO nanocomposite from bract extract of *Musa paradisiaca* for catalytic activity. Where, 96%, 93% and 91% degradation efficiencies are achieved from the organic dyes of MO, O-Nip and MB [20]. Kavita Sahu et al. [21] developed CuO/Cu_2O nanowire for catalytic reduction of 4-nitrophenol within 4 min due to their large surface area leading to enhanced adsorption and enhanced charge carrier separation. Nasrollahzadeh et al. reported Cu/Al_2O_3 nanoparticles were developed by leaf extract of *Commersonia Bartramia* for catalytic reduction of Methylene blue and Congo red in aqueous medium [22].

The Rhodamine B (RhB) dye is a cationic xanthene class dye and it has been used as textile and food industries. The Malachite green (MG) is widely used as a coloring agent in silk, jute, wool, paper for textile and leather industries and applied in aquaculture as a parasiticide and antibacterial agent. However, MG is toxic and carcinogenic. The wastewater containing MG causes environmental pollution and threats to human health. Thus, it is significant to eliminate MG from wastewater before its discharge [23]. Hence, catalytic activity has been investigated by Malachite green (MG) and Rhodamine B (RB) organic dyes from the developed catalyst of CuO/ZnO and CuO/CdO NCs via a two-step approach. The CuO NPs were prepared by the co-precipitation approach and subsequently, CuO/ZnO and CuO/CdO NCs were developed from the hydrothermal method.

2. Experimental procedure

2.1. Materials for synthesizing of CuO NPs, CuO/ZnO and CuO/CdO NCs

The precursor material of Copper chloride ($CuCl_2$), Zinc acetate ($Zn(CH_3CO_2)_2$) and Cadmium acetate ($Cd(CH_3CO_2)_2$) were used to develop the CuO NPs, CuO/ZnO and CuO/CdO NCs. The sodium borohydride ($NaBH_4$) performs as a reducing agent. In overall experimental studies, Double Distilled (DD) water is used as a solvent. All the chemicals and organic dyes (Rhodamine B and Malachite Green) were bought from Merk.

2.2. Synthesis procedure of CuO NPs, CuO/ZnO and CuO/CdO NCs

The pure CuO NPs were developed via a co-precipitation approach as per our previous report [3]. To prepare CuO/ZnO and CuO/CdO NCs, each 0.5 gm of prepared CuO NPs was added gradually into every 50 ml of DD water under sonication (15 min). Subsequently, each 0.05 M of CTAB was added into the above-prepared solution under constant stirring process. Later that, 0.1 M of $Zn(CH_3CO_2)_2$ was added into one of the solutions and 0.1 M of $Cd(CH_3CO_2)_2$ was mixed with another prepared solution. Then, the NaOH solution was added with the above prepared both solutions until pH 9 was reached. After that, the above-prepared solutions were changed into 100 ml of autoclave (Teflon-lined stainless steel) and heated at 140 °C for 12 h. Later, attained samples were collected and washed thoroughly into ethanol and DD water. After the washing process, the obtained material was heated at 90 °C and annealed at 300 °C for 2 h. Finally, CuO/ZnO and CuO/CdO NCs were collected for further analytical studies.

2.3. The catalytic activity test for RhB and MG

The organic dyes of Rhodamine B (1×10^{-3} M) and Malachite Green (1×10^{-5} M) were taken in 100 ml of DD water for an estimate of the catalytic activity of CuO/ZnO NCs and CuO/CdO NCs. Then, 10 mg of CuO/ZnO NCs and CuO/CdO NCs was added into RhB and MG solutions, separately. After that, the required amount of prepared $NaBH_4$solution (1×10^{-2} M) was added to the above mixture solution at room temperature. During the reaction, the reduction of dyes was observed from the intensity of wavelength was linearly decreased with respect to time intervals (30 s for RhB and 2 min for MG), which were recorded by UV–Vis spectrophotometer.

2.4. Analytical techniques

The PXRD pattern of synthesized pure CuO, CuO/ZnO and CuO/CdO NCs were analyzed by the Pro Penalty CAL (Cu-Kα radiation (1.5406 Å)) instrument model. The UV–Visible absorption spectra of developed samples were taken from the JASCO V-670 spectrophotometer. From the Zeiss Gemini Ultra-55 instrument model, FESEM and EDAX color mapping analysis were identified.

3. Results and discussion

3.1. Powder X-ray diffraction (PXRD) analysis

The PXRD pattern of (a) pure CuO, (b) CuO/ZnO and (c) CuO/CdO NCs were shown in Fig. 1. The major diffraction peaks are obtained at the 2θ values of 32.65°, 35.64°, 38.81°, 48.80°, 53.63°, 58.43°, 61.61°, 66.31°, 68.15°, 72.58° and 75.17° respectively for the planes of (110), (002), (111), (−202), (020), (202), (−113), (−311), (220), (311) and (−222), which are clearly reflect the monoclinic phase of CuO and good agreement with the standard reported JCPDS NO: 05–0661 [24,25]. The intensity peak positioned at 2θ of 31.79°, 34.28°, 36.20°, 47.36°, 56.51° and 62.76° is corresponding to the crystal planes of (100), (002), (101), (102), (110) and (103), respectively for hexagonal wurtzite phase structure of ZnO [JCPDS Card No 36–1451] [26]. The cubic phase structure of CdO has crystal planes (111), (200), (220), (311) and (222) with respective intensities at 33.02°, 38.33°, 55.15°, 65.83° and 69.30°, which are well coincided with the JCPDS No: 73–2245 [27]. The average crystallite sizes of the CuO, CuO/ZnO and CuO/CdO NCs were estimated by following Debye-Scherrer's formula.

$$D = K\lambda/\beta \cos\theta$$

where, 'D' and 'K' is Debye-Scherrer's crystallite size and constant, 'λ' represents the incident wavelength of the X ray's, 'β' and 'θ' denotes the full-width half maximum of the XRD corresponding

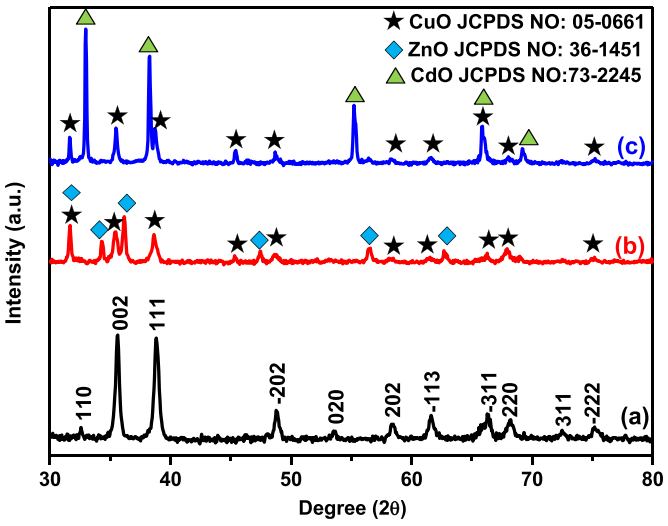

Fig. 1. PXRDpattern of (a) CuO, (b) CuO/ZnO NCs and CuO/CdONCs.

peaks and Bragg angle [3,26]. The average crystallite size is found to be 32 nm, 44 nm and 57 nm, respectively for pure CuO, CuO/ZnO and CuO/CdO NCs. The presence of defects in the developed materials was established by dislocation density (δ), which was determined by the given relation.

$$\delta = 1/D^2$$

The dislocation density (δ) of the pure CuO, CuO/ZnO and CuO/CdO NCs were attained to be 9.76×10^{-4} nm^{-2}, 5.16×10^{-4} nm^{-2} and 3.07×10^{-4} nm^{-2}, respectively [26]. From the result, the defects of the NCs materials are reduced than pure due to its surface charge properties.

3.2. Optical absorption studies

The UV–Vis spectrum of pure, CuO/ZnO and CuO/CdO NCs had been recorded in the visible range (Fig. 2). From the absorption spectra, band around between 200 nm and 300 nm for CuO and 366 nm, 372 nm respectively for ZnO and CdO. The maximum absorbance (366 nm and 372 nm) is assigned by the intrinsic band-gap adsorption of CuO/ZnO and CuO/CdO NCs owing to the electron transitions from the valence band to conduction band [9]. According to the maximum level band absorption, the band-gap energy of the pure, CuO/ZnO and CuO/CdO NCs was estimated based on the given Tauc's equation,

$$(\alpha h\upsilon)^2 = A\,(h\upsilon - Eg)$$

where, α, hυ & A is absorption coefficient, photon energy and Constant related to the effective mass of the electrons. The band-gap energy (Eg) is achieved to be 1.7 eV, 2.8 eV and 2.75 eV respectively for pure, CuO/ZnO and CuO/CdO NCs (Fig. 3a–c). From the result, the bandgap of the prepared NCs was a good agreement with the previously reported values [9,28].

3.3. Morphological analysis

The FESEM images of CuO/ZnO and CuO/CdO NCs were shown in Fig. 4(a–c) and Fig. 5(a–c). The attained particles of the synthesized CuO/ZnO and CuO/CdO NCs are seemed as spherical and stone-like morphology. From the observed figure, CuO/ZnO NCs have a uniform distribution of the particles and it has a large surface area compared to CuO/CdO NCs. The catalytic activity has been enhanced by these types of materials. Fig. 8(a–c) reveals that the TEM analysis of CuO/ZnO NCs. The average particle size ranges around 50–200 nm approximately from the developed CuO/ZnO NCs. The EDAX color mapping of CuO/ZnO and CuO/CdO NCs (Fig. 6 and Fig. 7) demonstrates additional support in the statement of individual atoms are evenly distributed with a combined ratio throughout the composite matrix of CuO/ZnO and CuO/CdO NCs. The color mapping clearly reveals only elements of Cu, Cd, Zn, and O were a presence in the developed composite materials.

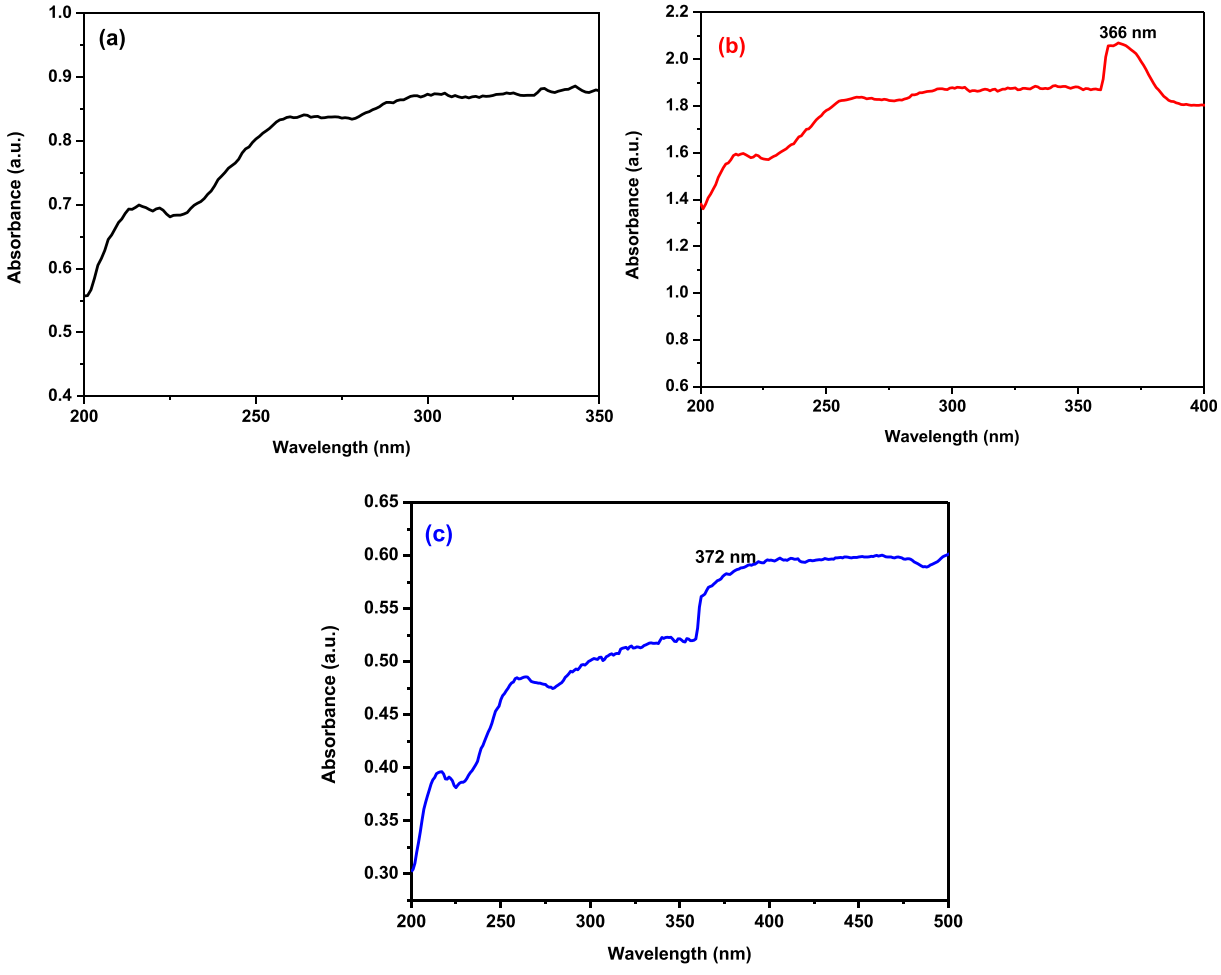

Fig. 2. UVVisible absorption spectrum of (a) CuO, (b) CuO/ZnO NCs and CuO/CdONCs.

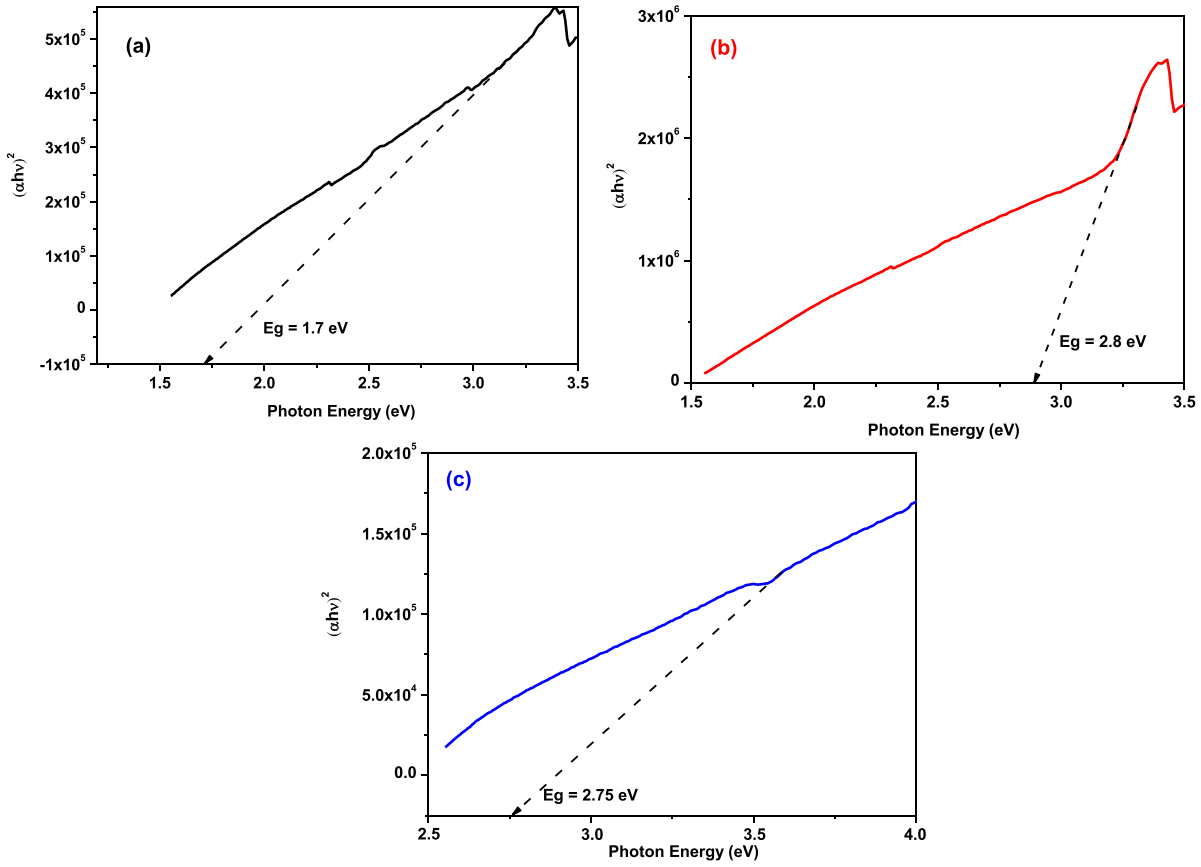

Fig. 3. Tauc's plot of (a) CuO, (b) CuO/ZnO NCs and CuO/CdONCs.

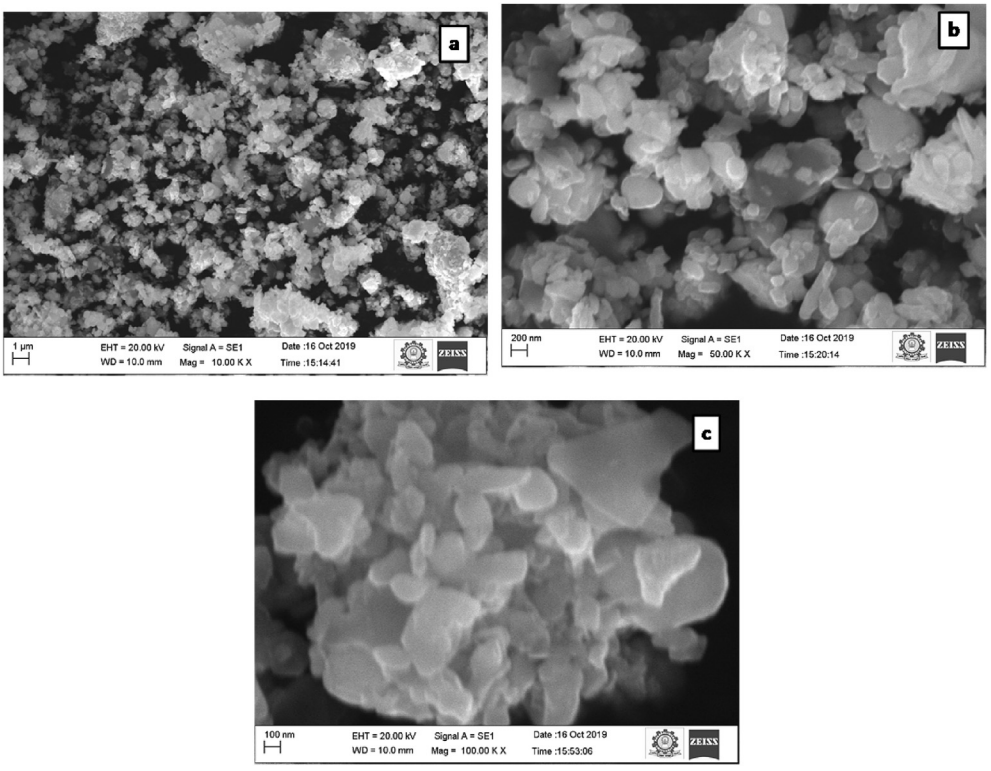

Fig. 4. Different magnification FESEM images of (a–c) CuO/ZnO NCs.

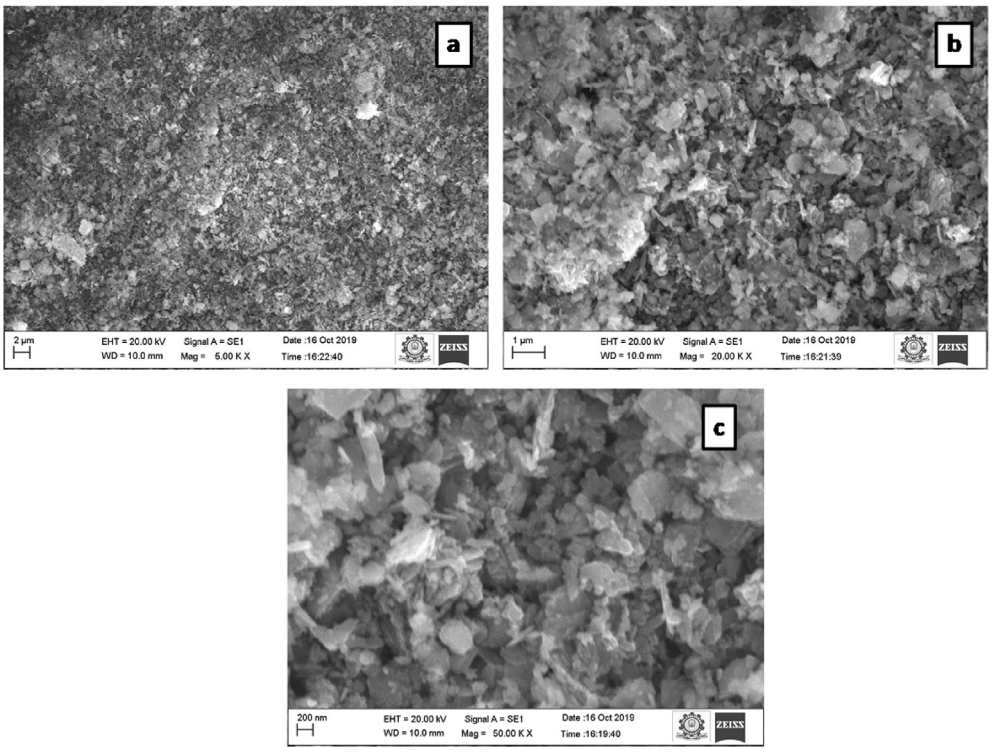

Fig. 5. Different magnification FESEM images of (a–c) CuO/CdO NCs.

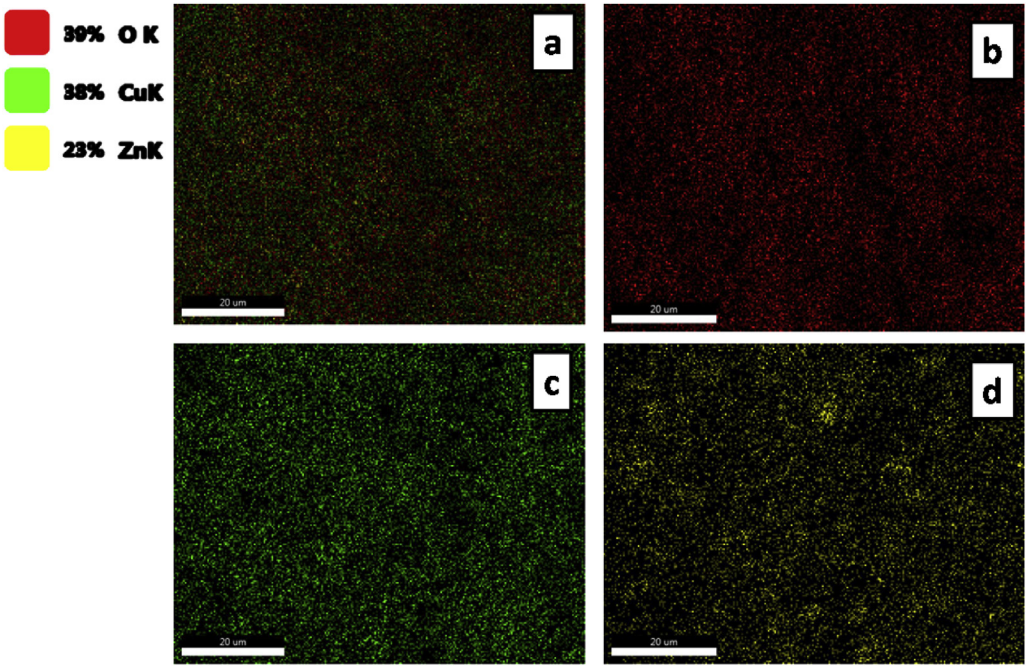

Fig. 6. EDAX color mapping images of (a–d) CuO/ZnO NCs.

3.4. Catalytic activity of RhB and MG for CuO/ZnO NCs and CuO/CdO NCs

The catalytic performance of RhB has been investigated by the prepared catalyst of CuO/ZnO and CuO/CdO NCs. In the catalytic activity, $NaBH_4$ acts as a reducing agent which is monitored by UV–Visible absorption spectra at different time intervals (Fig. 9). The reduction rate of RhB has no change by the absence of catalyst which suggesting that it is very difficult for the reduction of RhB without any catalyst. Therefore, the reduction rate of the RhB was increased in addition of CuO/ZnO and CuO/CdO nanocatalyst with $NaBH_4$ for degradation of RhB and the strong absorption intensity peak located at 554 nm rapidly decreases along with deep pink color solution change to colorless solution completely in 180 s due

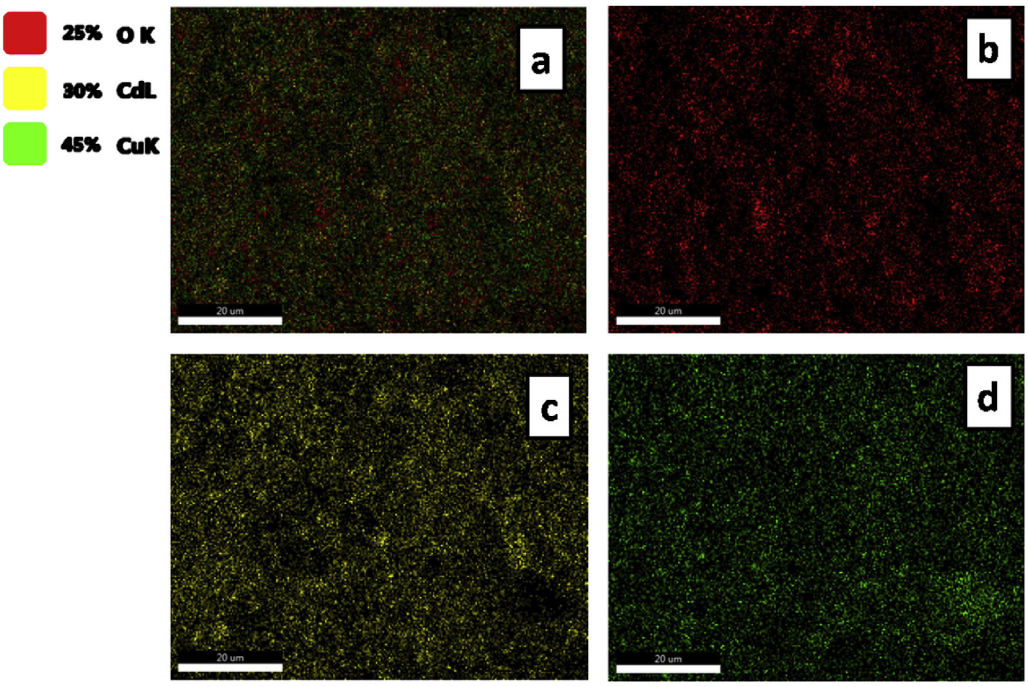

Fig. 7. EDAXcolor mapping images of (a–d) CuO/CdO NCs.

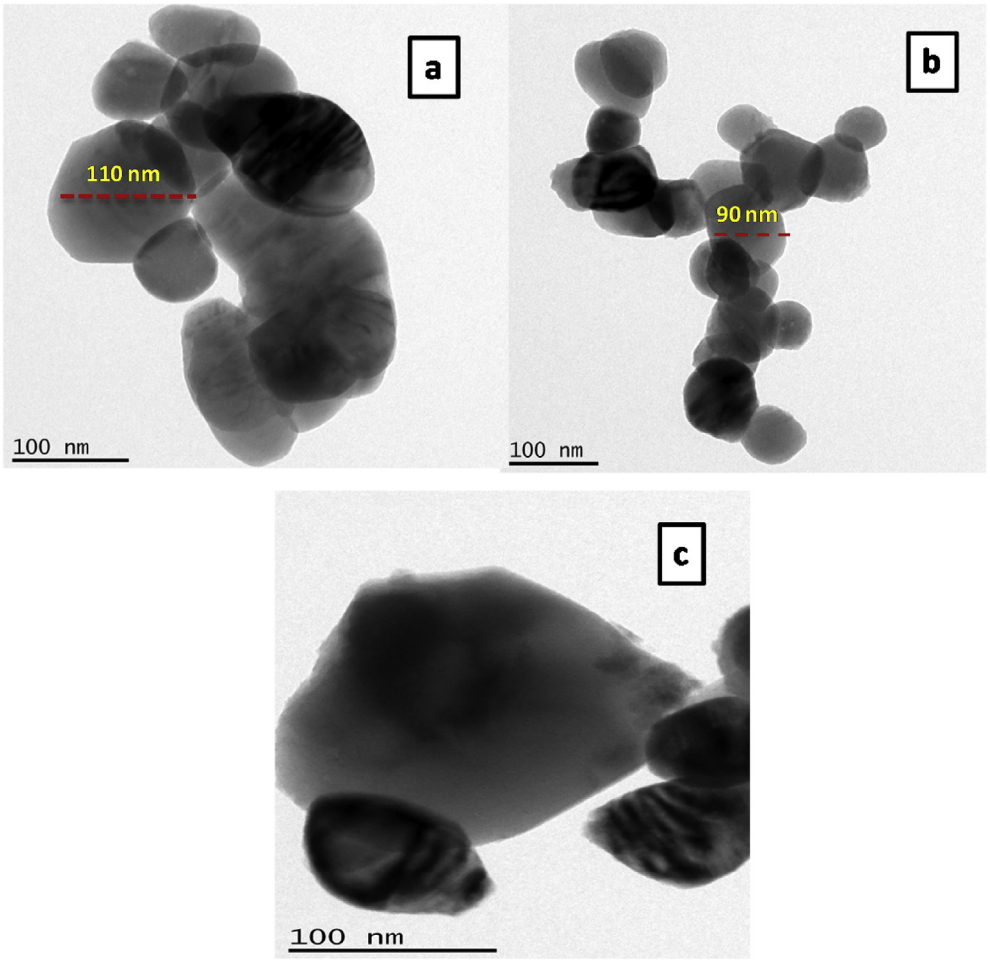

Fig. 8. Different magnification TEM images of (a–c) CuO/ZnO NCs.

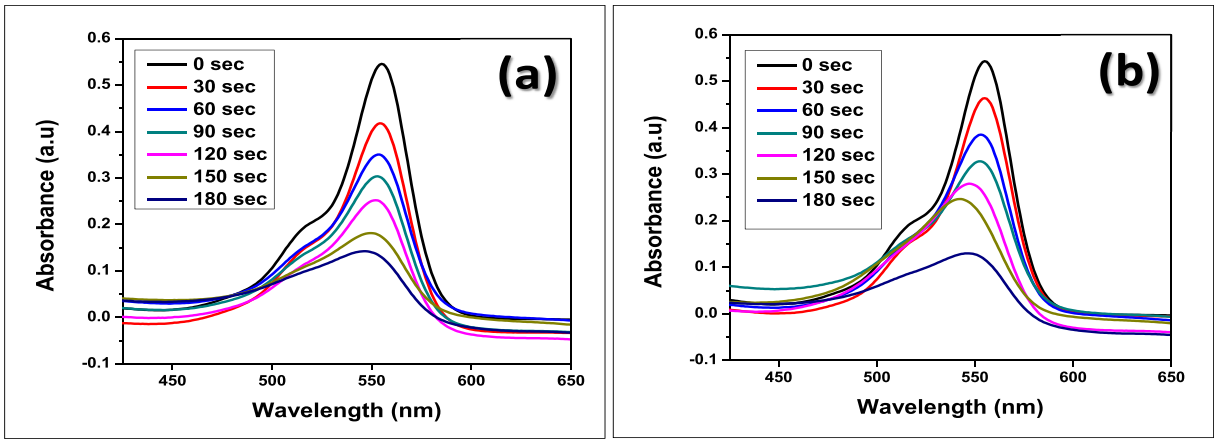

Fig. 9. Time-dependent UV–Vis absorption spectra for the catalytic reduction of MG (a) CuO/ZnO NCs and (b) CuO/CdO NCs.

to conversion of RhB (Pink color) into Leuco-RhB (colorless). The prepared catalyst of CuO/ZnO and CuO/CdO NCs were performance as an electron relay and supporting electron transfer from ions (donor) into RhB dye (acceptor). During the catalysis process, nucleophilic ions donate the electrons to the prepared catalyst, whereas electrophilic ions (RhB) capture the electrons from the catalyst [29,30].

Fig. 10 shows the reduction absorption spectra of MG with $NaBH_4$ by (a) CuO/ZnO and (b) CuO/CdO NCs. From the spectra, the high-intensity peak at 615 nm of MG was linearly decreased within 12 min due to the conversion of MG (green color) into leucomalachite green (LMG) (colorless). Here, CuO/ZnO and CuO/CdO NCs act as an important electron transfer mediator because it allows the electrons from $NaBH_4$ and donates to MG by acting as redox catalyst, which in turn termed as electron relay effect [31,32]. The catalytic behavior for the reduction of MG and RhB dyes are dependent on the efficient separation of charge carriers and surface area of the catalyst [29,30]. Further, heterojunction nanostructures of $SiO_2/Ag_2O/TiO_2$ have superior catalytic activity by the reduction of 4-NP to 4-AP owing to the heterojunction structure, which improves charge separation [33]. Sahu et al. developed CuO/Cu_2O hybrid nanowires for the reduction of 4-NP to 4-AP due to their large surface area and separation of charge carrier [20]. The RhB and MG results were compared with previous reports which are shown in Table 1.

Table 1
Comparison of catalytic activity CuO/ZnO and CuO/CdO NPs with some reported catalyst in the degradation of RhB and MG.

Catalyst	Dyes	Time (sec)	Rate constant(k)	Ref.
CuO/rGO	4-NP	27 min	13.951 min^{-1}	[34]
$Ni(OH)_2$	RhB	13 min	1.3×10^{-2} min^{-1}	[30]
ZnO/MgO	MO	14 min	8.39×10^{-3} s^{-1}	[19]
	MB	12 min	4.43×10^{-3} s^{-1}	
$Au/CeO_2–TiO_2$	RhB	10 min	223.9×10^{-3} min^{-1}	[35]
	MG	14 min	233.2×10^{-3} min^{-1}	
PET2-APTES-Ag/Cu	MG	9 min	0.145 min^{-1}	[36]
$CuO/TiO_2/ZnO$	4-NP	360 s	8.13×10^{-2} s^{-1}	[37]
	MB	210 s	1.351×10^{-2} s^{-1}	
	CV	135 s	1.262×10^{-2} s^{-1}	
CuO/ZnO	RhB	180 s	7.23×10^{-3} s^{-1}	Present work
	MG	180 s	1.29×10^{-2} s^{-1}	
CuO/CdO	RhB	180 s	6.30×10^{-3} s^{-1}	Present work
	MG	180 s	1.13×10^{-2} s^{-1}	

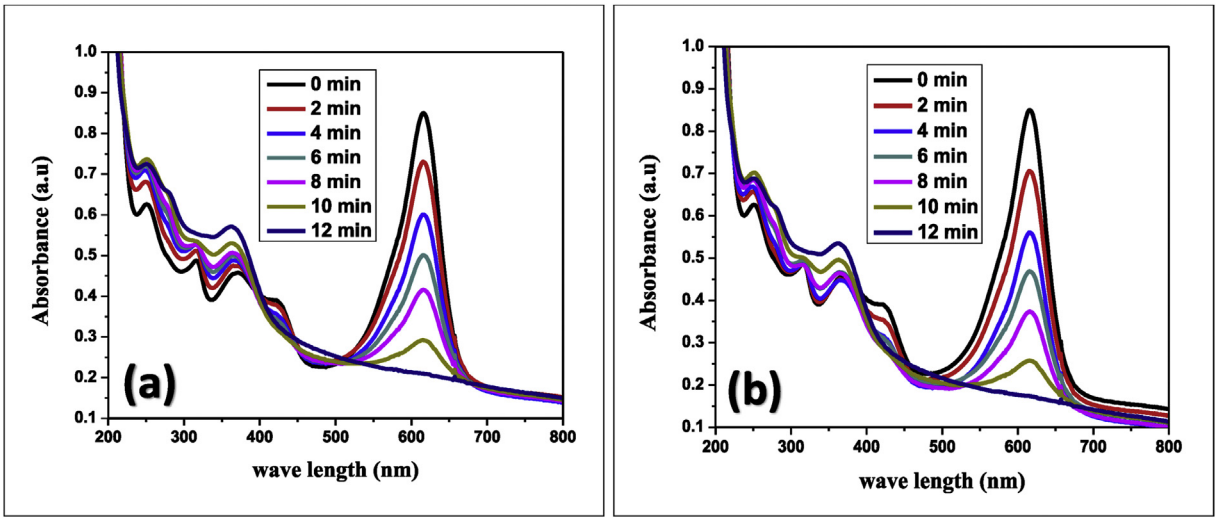

Fig. 10. Time-dependent UV–Vis absorption spectra for the catalytic reduction of RhB (a) CuO/ZnO NCs and (b) CuO/CdO NCs.

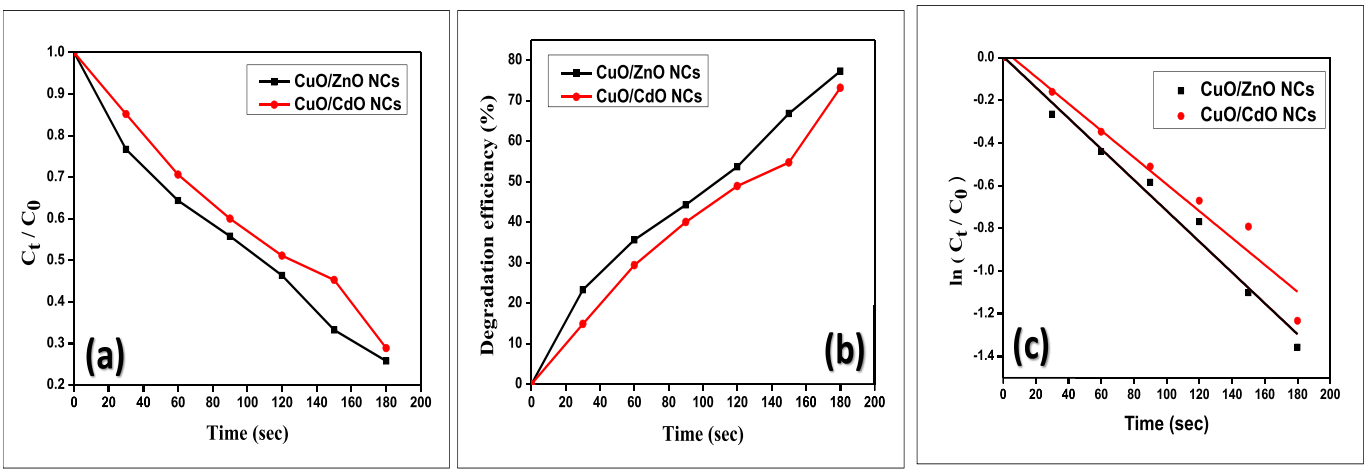

Fig. 11. (a) Plots of C_t/C_0 versus reaction time (sec), (b) MG Degradation efficiency (%) versus reaction time (sec) and (c) ln (C_t/C_0) versus reaction time (sec) for CuO/ZnO NCs and CuO/CdO NCs.

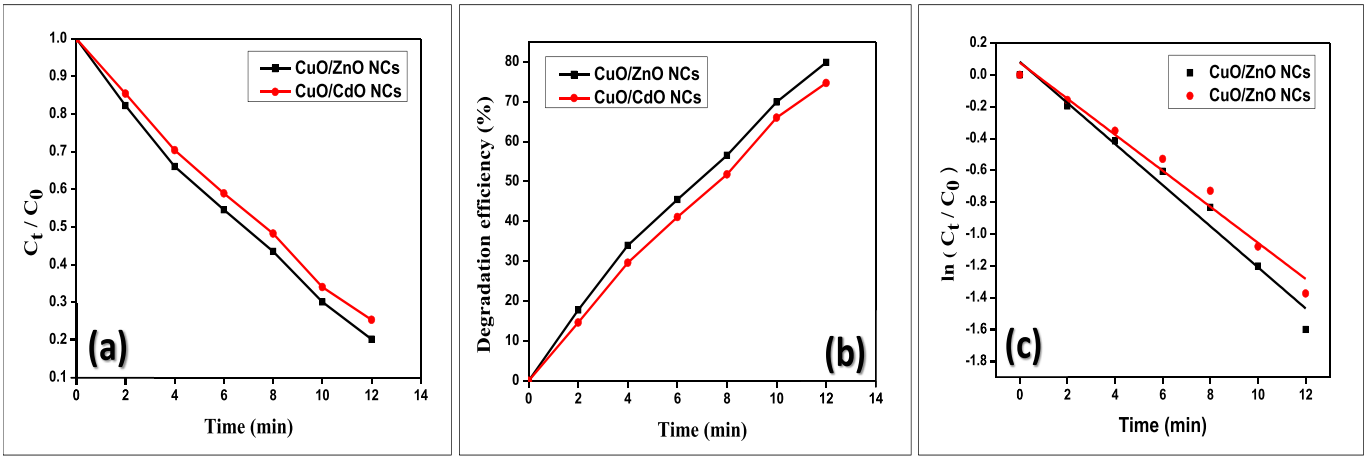

Fig. 12. (a) Plots of C_t/C_0 versus reaction time (sec), (b) RhB Degradation efficiency (%) versus reaction time (sec) and (c) ln (C_t/C_0) versus reaction time (sec) for CuO/ZnO NCs and CuO/CdONCs.

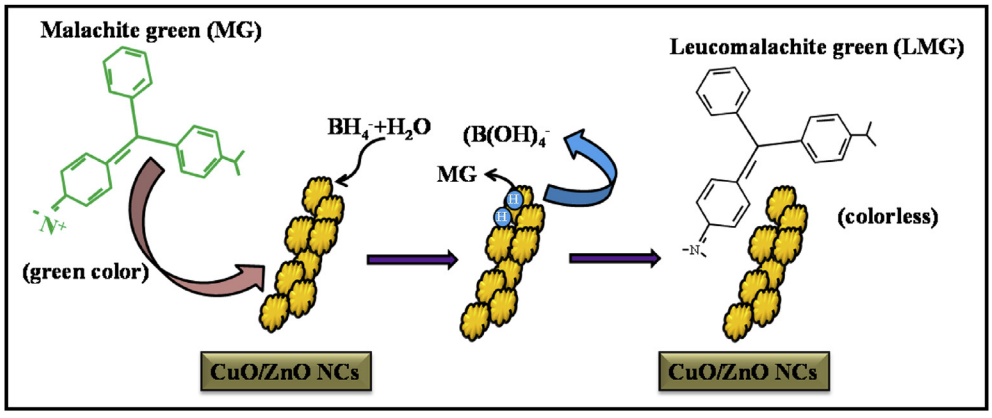

Fig. 13. Possible reduction mechanism of malachite green (MG) into leucomalachite green (LMG) in presence of CuO/ZnO NCs.

3.5. The reaction kinetics of RhB and MG for CuO/ZnO NCs and CuO/CdO NCs

Figs. 11a and 12(a) reveals that the C_t/C_0 versus reaction time (t) for the degradation of RhB and MG dye from the catalyst of CuO/ZnO and CuO/CdO NCs. The dye degradation efficiency can be determined by the given relation

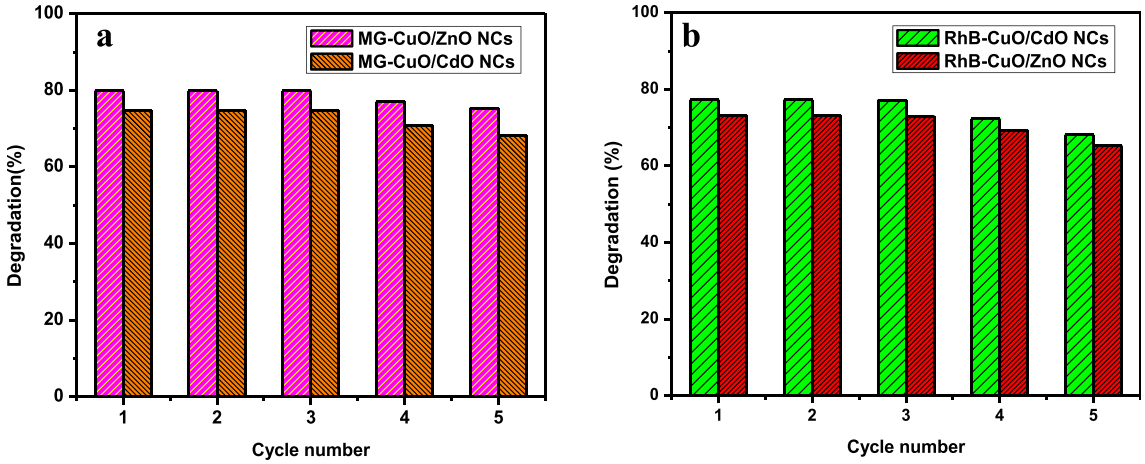

Fig. 14. (a & b) The recyclability of the catalyst in the reduction of MG and RhB dye solution with $NaBH_4$ at room temperature.

$$R = [(C_0 e C_t) / C_0] \times 100\ \%$$

where, C_0 and C_t are initial and final concentrations with respect to time 't' and '0' respectively for RhB and MG. The degradation efficiency of RhB and MG for CuO/ZnO and CuO/CdO NCs are plotted with time and depicts in Figs. 11 (b) and 12 (b). The degradation efficiency of CuO/ZnO and CuO/CdO NCs are found to be 77.26%, 73.15% for RhB and 79.82%, 74.69 for MG, respectively. From the observed result, CuO/ZnO NCs catalyst increases the reduction rate of MG dye compare to CuO/CdO NCs due to their large surface area of the adsorption of MG anions, which leads to an increase in the catalytic activity. The rate constant for the reduction of dyes was estimated by pseudo-first-order kinetics [20]. The kinetic reaction can be determined from the given equation

$$\ln (C_t / C_o) = kt$$

where C_t and C_o are the final and initial concentration of RhB and MG and 'k' denotes the rate constant at the given reaction time (t). From Figs. 11 (c) and 12 (c) demonstrates that the difference of ln C_t/C_o against reaction time for the degradation of RhB and MG for CuO/ZnO and CuO/CdO NCs. The rate constant (k) of CuO/ZnO and CuO/CdO NCs are determined from the linear slope value and found to be $7.23 \times 10^{-3}\ s^{-1}$ and $6.30 \times 10^{-3}\ s^{-1}$ for RhB, $1.29 \times 10^{-2}\ s^{-1}$and $1.13 \times 10^{-2}\ s^{-1}$ for MG respectively. The (R^2) values of CuO/ZnO and CuO/CdO NCs are calculated to be 0.9823 and 0.9580 for RhB, 0.9746 and 0.9207 for MG, respectively. From the result, the degradation efficiency and rate constant of CuO/ZnO are high in the degradation of both dyes. The possible reduction mechanism of malachite green (MG) into leucomalachite green (LMG) in the presence of CuO/ZnO NCs were shown in Fig. 13.

3.6. Catalyst recyclability

In industrial applications, recycling of the catalyst is very essential. To estimate its reusability, CuO/CdO and CuO/ZnO NCs were performing with successive catalytic tests. After each catalytic test, the used CuO/CdO and CuO/ZnO NCs were washed by water and dried at room temperature**.** Although, CuO/ZnO NCs reveals high catalytic activity than CuO/CdO NCs, they were reused for five consecutive cycles to degrade RhB which is achieved to be 68.13 and 65.32% degradation efficiency. The presence of CuO/ZnO NCs catalyst, MG degradation achieved in recycling efficiency of 75.32% and 68.15%, respectively. After five consecutive rounds, degradation efficiency was rapidly reduced owing to their dye molecules are extremely adsorbed from the surface area (Fig. 14) [37].

4. Conclusion

The CuO/CdO and CuO/ZnO NCs were developed via the two-step approach. The CuO prepared by the co-precipitation method and subsequently ZnO and CdO were developed from a hydrothermal approach for catalytic activity. From the Powder X-ray diffraction (PXRD) analysis, crystalline sizes were achieved to be 32 nm, 44 nm and 57 nm respectively for pure CuO, CuO/ZnO and CuO/CdO NCs. The spherical and stone-like morphology was attained by the developed composite material and individual atoms are evenly distributed with a combined ratio throughout the composite matrix of CuO/ZnO and CuO/CdO NCs, which were primarily confirmed by the EDAX color mapping. In catalytic degradation studies, the degradation efficiency and rate constant of CuO/ZnO NCs are high at both the dyes due to their large surface area and separation of charge carrier. In the recyclable test, catalytic activity loss was observed after five consecutive rounds owing to their dye molecules are extremely adsorbed from the surface area. The better catalytic property of the material reveals that it is applicable to remove the environmental pollutants released from the industries.

CRediT authorship contribution statement

A. Sankaran: Conceptualization, Methodology, Validation, Writing - review & editing. **K. Kumaraguru:** Resources, Investigation, Writing - original draft, Supervision.

References

[1] S. Jagadhesan, N. Senthilkumar, V. Senthilnathan, T.S. Senthil, Sb doped ZnO nanostructures prepared via co-precipitation approach for the enhancement of MB dye degradation, Mater. Res. Express 5 (2018) 205040.
[2] M. Jayapriya, M. Arulmozhi, B. Balraj, Fabrication of silver nanoparticles using Musa aradisiacal for its synergistic combating effect on Phytopathogens and free radical scavenging activity, IET Nanobiotechnol. 13 (2019) 134–143.
[3] A. Pramothkumar, N. Senthilkumar, K.C. Mercy Gnana Malar, M. Meena, I. Vetha Potheher, A comparative analysis on the dye degradation efficiency of pure, Co, Ni and Mn-doped CuO nanoparticles (2019) 19043–1905, J. Mater. Sci. Mater. Electron. 30 (2019).
[4] M.K. Satheesan, K. Vani, Viswanathan Kumar, Acceptor-defect mediated room temperature ferromagnetism in (Mn^{2+}, Nb^{5+}) co-doped ZnO nanoparticles, Ceram. Int. 43 (2017) 8098–8102.
[5] R. Sahay, J'Sundaramurthy, P.S. Kumar, V. Thavasi, S.G. Mhaisalkar, S. Ramakrishna, Synthesis and characterization of CuO nanofibers, and

investigation for its suitability as blocking layer in ZnO NPs based dye sensitized solar cell and as photocatalyst in organic dye degradation, J. Solid State Chem. 186 (2012) 261–267.
[6] C.C. Vidyasagar, Y. ArthobaNaik, T.G. Venkatesh, R. Viswanathan, Solid-state synthesis and effect of temperature on optical properties of Cu–ZnO, Cu–CdO and CuO nanoparticles Powder Technol 214 (2011) 337–343.
[7] N. Senthil Kumar, M. Ganapathy, S. Sharmila, M. Shankar, M. Vimalan, I. VethaPotheher, ZnO/Ni(OH)$_2$ core-shell nanoparticles: synthesis, optical, electrical and photoacoustic property analysis, J. Alloys Compd. 703 (2017) 624–632.
[8] S. Sitthichai, A. Phuruangrat, T. Thongtem, S. Thongtem, Influence of Mg dopant on photocatalytic properties of Mg-doped ZnO nanoparticles prepared by sol–gel method, J. Ceram. Soc. Japan 125 (2017) 122–124.
[9] G. Somasundaram, J. Rajan, J. Paul, Effect of the calcination process on CdO–ZnO nanocomposites by a honey-assisted combustion method for antimicrobial performance, Toxicology Res 7 (2018) 779–791.
[10] M. Jayapriya, M. Arulmozhi, B. Balraj, Optical, biological and catalytic properties of ZnO incorporated MgO nanostructures using Musa paradisiaca bract extract, Ceram. Int. 44 (2018) 13152–13160.
[11] A. O Juma, E.A. Arbab, C.M. Muiva, L.M. Lepodise, G.T. Mola, Synthesis and characterization of CuO-NiO-ZnO mixed metal oxide nanocomposite, J. Alloys Compd. 723 (2017) 866–872.
[12] L.Y. Lin, B.B. Karakocak, S. Kavadiya, T. Soundappan, P. Biswas, A highly sensitive non-enzymatic glucose sensor based on Cu/Cu$_2$O/CuO ternary composite hollow spheres prepared in a furnace aerosol reactor, Sensor. Actuator. B Chem. 259 (2018) 745–752.
[13] H. Sudrajat, S. Hartuti, Structural properties and catalytic activity of a novel ternary CuO/gC_3N_4/Bi_2O_3photocatalyst, J. colloid. interf. sci. 524 (2018) 227–235.
[14] Y. Chen, D. Liu, L. Yang, M. Meng, J. Zhang, L. Zheng, S. Chu, T. Hu, Ternary composite oxide catalysts CuO/Co_3O_4–CeO_2 with wide temperature-window for the preferential oxidation of CO in H_2-rich stream, Chem. Eng. J. 234 (2013) 88–98.
[15] A.K. Sasmal, S. Dutta, T. Pal, A ternary Cu_2O–Cu–CuOnanocomposite: a catalyst with intriguing activity, Dalton Trans. 45 (2016) 3139–3150.
[16] B. Durán, S.A. Hevia, L. Molero, M. Isaacs, S. Bonardd, D.D. Diaz, A. Leiva, C. Saldías, Novel 3D copper nanoparticles/chitosan/nanoporous alumina (CCSA) membranes with catalytic activity Characterization and performance in the reduction of methylene blue, J. Clean. Prod. 210 (2019) 811–820.
[17] E. Gomathi, B. Balraj, K. Kumaraguru, Electrochemical degradation of scarlet red dye from aqueous environment by titanium based dimensionally stable anodes with SS electrodes, Springer - Applied Biological Chemistry 61 (2017) 289–293.
[18] S. Jain, S. Mishra, T.K. Sarma, Zn^{2+} induced self-assembled growth of octapodal Cu_xO–ZnO microcrystals: multifunctional applications in reductive degradation of organic pollutants and nonenzymatic electrochemical sensing of glucose, ACS Sustain. Chem. Eng. 6 (2018) 9771–9783.
[19] K. Sahu, B. Satpati, R. Singhal, S. Mohapatra, Enhanced catalytic activity of CuO/Cu_2O hybrid nanowires for reduction of 4-nitrophenol in water, J. Phys. Chem. Solid. 136 (2020) 109143.
[20] J. Maruthai, A. Muthukumarasamy, B. Baskaran, Optical, biological and catalytic properties of ZnO/MgO nanocomposites derived via Musa paradisiaca bract extract, Ceram. Int. 44 (2018) 13152–13160.
[21] N. Sreeju, A. Rufus, D. Philip, Studies on catalytic degradation of organic pollutants and anti-bacterial property using biosynthesized CuO nanostructures, J. Mol. Liq. 242 (2017) 690–700.
[22] M. Nasrollahzadeh, Z. Issaabadi, S.M. Sajadi, Green synthesis of Cu/Al_2O_3 nanoparticles as efficient and recyclable catalyst for reduction of 2, 4-dinitrophenylhydrazine, Methylene blue and Congo red Composites, Pa. Birds: Eng. Times 166 (2019) 112–119.
[23] J. Yang, X. Xu, Y. Liu, Y. Gao, H. Chen, H. Li, Preparation of SiO_2@TiO_2 composite nanosheets and their application in photocatalytic degradation of malachite green at emulsion interface, Colloid. Surface. Physicochem. Eng. Aspect. 582 (2019) 123858.
[24] N.M. Basith, J.J. Vijaya, L.J. Kennedy, M. Bououdina, Structural, optical and room-temperature ferromagnetic properties of Fe-doped CuO nanostructures, Phys. E 53 (2013) 193–199.
[25] E. Nandhakumar, P. Priya, P. Selvakumar, E. Vaishnavi, A. Sasikumar, N. Senthilkumar, One step hydrothermal green approach of CuO/Ag nanocomposites: analysis of structural biological activities, Mater. Res. Express 6 (2019), 095036.
[26] N. Senthilkumar, M. Ganapathy, A. Arulraj, M. Meena, M. Vimalan, I. VethaPotheher, Two step synthesis of ZnO/Ag and ZnO/Au core/shell nanocomposites: structural, optical and electrical property analysis, J. Alloys Compd. 750 (2018) 171–181.
[27] K. Usharani, R. Balu, V.S. Nagarethinam, M. Suganya, Characteristic analysis on the physical properties of nanostructured Mg-doped CdO thin films—doping concentration effect, Progress Nat. Sci. Mater. Int. 25 (2015) 251–257.
[28] Nthambeleni Mukwevho, Elvis Fosso-Kankeu, Frans Waanders, Neeraj Kumar, Suprakas Sinha Ray, Xavier YangkouMbianda, Photocatalytic activity of $Gd_2O_2CO_3$·ZnO·CuO nanocomposite usedfor the degradation of phenanthrene, SN Applied Sci 1 (2019) 10.
[29] P.C. Nagajyoyhi, K.C. Devarayapalli, T.V.M. Sreekanth, S.V. PrabhakarVattikuti, Jaesool Shim, Effective catalytic degradation of rhodamine B using $ZnCO_2O_4$ nanodice, Mater. Res. Express 6 (10) 105069.
[30] P.C. Nagajyothi, K.C. Deyarayapalli, C.O. Tettey, S.V. PrabhakarVattikuti, Jaesool Shim, Eco-friendly green synthesis: catalytic activity of nickel hydroxide nanoparticles, Mater. Res. Express 6 (2019), 055036.
[31] M. Bordbar, N. Negahdar, M. Nasrollahzadeh, M. Officinalis L. leaf extract assisted green synthesis of CuO/ZnO nanocomposite for the reduction of 4-nitrophenol and Rhodamine B, Separ. Purif. Technol. 191 (2018) 295–300.
[32] Balakumar Vellaichamy, Periakaruppan Prakash, Ag nanoshellcatalyzeddedying of industrial effluents, RSC Adv. 6 (2016) 31653–31660.
[33] O.A. Zelekew, D.H. Kuo, A two-oxide nanodiode system made of double-layered p type Ag_2O@n-type TiO_2 for rapid reduction of 4-nitrophenol, Phys. Chem. Chem. Phys. 18 (2016) 4405–4414.
[34] Chandrama Sarkar, Swapan K. Dolui, Synthesis of copper oxide/reduced graphene oxide nanocomposite and its enhanced catalytic activity towards reduction of 4-nitrophenol, RSC Adv. 5 (2015) 60763–60769.
[35] Pranjal Saikia, A.B.U. T Miah, Partha P. Das, Highly efficient catalytic reductive degradation of various organic dyes by Au/CeO_2-TiO_2nano-hybrid, J. Chem. Sci. 129 (2017) 81–93.
[36] Bouazizi Nabil, Mohammad NeazMorshed, Campagne Christine BeharyNemeshwaree, Vieillard Julien, Thoumire Olivier, AzzouzAbdelkrim, Development of new multifunctional filter based nonwovens for organics pollutants reduction and detoxification: high catalytic and antibacterial activities, Chem. Eng. J. 356 (2019) 702–716.
[37] C. Mathalai Sundaram, S. Kalpana, S. Rafi Ahamed, V. Sivaganesan, E. Nandhakumar, Studies on the catalytic activity of CuO/TiO_2/ZnO ternary nanocomposites prepared via one step hydrothermal green approach, Mater. Res. Express 6 (2019) 125043.